Energy Conversion and Management 188 (2019) 438–446

Contents lists available at ScienceDirect

Energy Conversion and Management

journal homepage: www.elsevier.com/locate/enconman

Power generation enhancement in direct methanol fuel cells using non-uniform cross-sectional serpentine channels

Xu-Qu Hu[a], Qin-Wen Yang[a,*], Gang Xiao[a,b,1], Xiao-Ting Chen[a,1], Xiang Qiu[c]

[a] State Key Laboratory of Advanced Design and Manufacturing for Vehicle Body, College of Mechanical and Vehicle Engineering, Hunan University, Changsha 410082, China
[b] CRRC Zhuzhou Institute Co., Ltd, Zhuzhou 412001, China
[c] School of Science, Shanghai Institute of Technology, Shanghai 201418, China

ARTICLE INFO

Keywords:
Direct methanol fuel cell
Flow-field design
Non-uniformity

ABSTRACT

Non-uniform cross-sectional designs of serpentine channel in direct methanol fuel cells are systematically studied in the present work. A parametric design is proposed to describe and classify channel geometries whose effects on cell performance are numerically and experimentally analyzed. Numerical results show that the non-uniform converging designs are beneficial for both in- and through-plane methanol transportations, and thus to enhance the peak power generation performance as much as 12% at high-current-density operations. Effectiveness of non-uniform designs for power generation enhancements is also validated by experimental studies which consider various operating conditions, and significant enhancement of power generation (18.4%) is noticed by the usage of non-uniform converging design. Optimal application conditions for the non-uniform converging designs are determined to be the high-current-density operations with high temperatures.

1. Introduction

Direct methanol fuel cell (DMFC) is regarded as a promising power source for mobile applications attributing to its advantages of simple structure, rapid recharge and high energy density [1]. However, further improvements are still greatly needed for accelerating its commercializations [2]. In the past decade, lots of efforts have been contributed for power generation enhancements in DMFCs by optimizing the catalyst loading [3], proton exchange membrane (PEM) structure [4] and water management [5], etc.

For liquid feed DMFCs, the essential processes such as reactant supply and product removal are normally realized through anode flows. An appropriate design of anode flow fields is highly beneficial in improving the efficiencies of fuel supply, methanol distribution and CO_2 removal and thus to achieve DMFC performance enhancement [6]. Since the pioneering works initiated in 1990s [7], the design of anode flow fields has received increasing attention. Lots of flow-field designs were creatively proposed and comparatively investigated, including but not limited to the serpentine and parallel channels [8], the grid [9] or interdigitated [10,11] fields and the bio-inspired configurations [12,13].

Despite of the multiplicity of new designs that have emerged, the advantages of serpentine configuration have been continuously emphasized in previous literatures. It was shown to be able to depress methanol crossover [14], to improve velocity distribution uniformity [15], to increase methanol transport efficiency [16] and also to enhance power generations [17]. Attributing to these competitive advantages, the serpentine configuration has become one of the most popular flow-field designs [13], and its geometry optimizations have attracted considerable interest from both fundamental and practical points of view. One of the earliest studies on the geometric effects of anode serpentine channel on DMFC performance was performed by Yang and Zhao [18]. Their experimental results indicated that both open ratio and flow channel length had significant influences on the cell performance. Subsequent researches have elucidated the effects of channel depth [19,20], channel width [21], rib width and channel/rib aspect ratio [22,23] on the energy conversion performances of DMFCs. There is also growing evidence for the existence of optimal serpentine geometry for DMFC performance [24,25]. However, the majority of previous studies have assumed a constant cross-section for serpentine channel during geometry optimisations. The influence of non-uniform cross-sectional designs on DMFC performance has been ignored to some extent [26]. In recent years, the non-uniform cross-sectional designs for serpentine channels has begun to emerge. Certain non-uniform designs, such as

* Corresponding author.
E-mail address: yangqinwen@hnu.edu.cn (Q.-W. Yang).
[1] These authors contribute equally in this study.

https://doi.org/10.1016/j.enconman.2019.03.058
Received 3 December 2018; Received in revised form 18 March 2019; Accepted 19 March 2019
Available online 29 March 2019
0196-8904/

Table 1
Summary of common flow-filed designs in fuel cells.

Designs			Types	Ref.
Uniform	Parallel	Conventional configuration	DMFC	[18]
	Serpentine	Conventional configuration	DMFC	[18]
		Channel depth	DMFC/PEMFC	[19,20]
		Channel width	DMFC	[21]
		Rib width	DMFC/PEMFC	[22,23]
		Cross-section aspect ratio	PEMFC	[23]
Non-uniform	Bio-inspired	Leaf-like shape	DMFC	[12,13]
		Lung-like shape	DMFC	[12,13]
	Serpentine	Convergent/divergent depth	PEMFC	[27]
		Wavy width	PEMFC	[28]
		Streamline-graded structure	PEMFC	[29]

varying depth [27], wavy width [28] and converging and diverging shapes [29], were shown to provide considerable advantages in power generations for proton exchange membrane fuel cells (PEMFCs). However, the studies of non-uniform designs in DMFCs cannot be easily available till now (see Table 1). The underlying mechanism of non-uniform designs is still in great need for DMFC system designers. Moreover, the existing non-uniform designs normally involve complex geometries, which would make considerable difficulties in manufacturing or assembling process. A concise non-uniform design of serpentine channel in DMFCs thus becomes the initial motivation of the present work. And comprehensive study using numerical and experimental techniques is designed to investigate its coupling effects with operating conditions on the power generation performance. In the present study, non-uniform cross-sectional designs of serpentine configuration are firstly proposed (Section 2.1). In Sections 2.2 and 2.3, numerical model that is applied for the investigations of geometric effects on cell performance is described and experimentally validated. Numerical results of methanol concentration distribution, current density distribution and global power generation performance are carefully discussed in Section 3 to clarify the underlying mechanism of non-uniform designs. Thereafter, systematic experimental studies are performed to further validate the numerical revealings and also to clarify the optimal application conditions of non-uniform designs (Section 4). Conclusions are available in Section 5.

2. Methods and models

Systematic analysis about the effects of non-uniform cross-sectional design of serpentine channels on the power generation performance in DMFC systems is performed based on the collaborations of experimental and numerical techniques. The non-uniform cross-sectional designs (Section 2.1), the applied numerical model (Section 2.2) and its experimental validations (Section 2.3) are all presented in this section.

2.1. Non-uniform cross-sectional designs

Serpentine channels with uniform cross-section (Fig. 1(a)) have been regularly embedded in many DMFC systems, for which the cross-sectional area S is constant in both straight and U-turn sections. A parametric design of non-uniform channel cross-sections is proposed for serpentine configurations in the present study. Specifically, the cross-sectional area of each straight pass is considered to be gradually varied along the flow direction, while an area recovery is designed to occur at the U-turn sections, as shown in Fig. 1(b) and (c).

The variation of cross-sectional area is realized through the change of channel width, while the channel depth is kept to be constant. A variation ratio σ is introduced to quantify the geometrical change of channel cross-section, which is defined as,

$$\sigma = \frac{S_2}{S_1}, \tag{1}$$

where S_1 and S_2 indicate the upstream and downstream cross-sectional areas of each straight section. Therefore, the so-called "regular design" of uniform cross-section for serpentine channel can be represented by $\sigma = 1.0$ (Fig. 1(a)), while $\sigma < 1.0$ and >1.0 denote the converging and diverging designs, respectively, as shown in Fig. 1(b) or (c).

In the present study, a regular design ($\sigma = 1.0$) of serpentine channel of 22 channel passes (i.e., 21 U-turns) is selected as reference state according to our experimental experience [30–32]. The channel width and depth are designed to be 0.85 mm and 1 mm for the regular condition, respectively, while the corresponding active area of membrane electrolyte assembly (MEA) is 12.25 cm^2. Considering that the pass number, channel depth, MEA active area and upstream cross-sectional area S_1 are all kept the same as reference state, three non-uniform designs are proposed for comparative study of σ effects, i.e., $\sigma = 0.6$, 0.8, 1.25.

Detailed information about the four designs is summarised in Table 2. The channel volume and the open ratio (i.e., the ratio between the open area and the active area [33]), are both found to increase with the cross-sectional variation ratio σ. However, the effects of σ on power generation can not be simply determined from geometrical parameters. It deserves to be fully investigated, and systematic studies are thus performed using numerical techniques in the following sections.

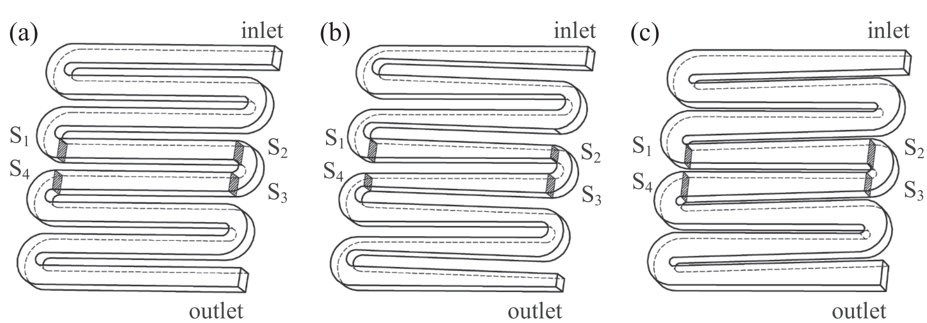

Fig. 1. Regular (a), convergent (b) and divergent (c) cross-sectional designs for serpentine channel.

Table 2
Geometrical parameters for the four main cross-sectional designs.

Variation ratio (σ)	Open ratio (%)	Channel volume (mm^3)	Info.
0.60	42.44	527.34	Converging
0.80	47.64	591.89	Converging
1.00	52.81	656.14	Regular
1.25	59.15	734.97	Diverging

2.2. Numerical model

A three-dimensional numerical model that couples the equations of species transport, mass and momentum conservations and the semi-empirical electro-chemical expressions was developed in our previous work to describe the energy conversion process in DMFC systems [30–32]. Relevant governing equations are summarised in A for convenience. It has shown a good agreement with experimental results from different DMFC systems, and was successfully applied to study the effects of different operating parameters and to derive an optimal operation strategy for voltage stability enhancement [31,32]. This well-constructed numerical model is adapted in the present study.

Numerical simulations are performed using a Computational Fluid Dynamics (CFD) code known as Fluent 16.0 which is based on the finite volume method. For regular design, its flow domain is discretized into structured grids consisting of 1146194 cells and 1343512 nodes. No-slip conditions are employed on boundary walls, and the conditions of velocity inlet and pressure outlet are defined at the inlet and outlet of flow channel. Operating parameters are set as experimental conditions. Governing equations of this incompressible flow can be solved by the implicit and pressure-based solver, and the pressure–velocity coupling is processed using SIMPLE algorithm. Numerical computations are considered to be steady and terminated when the current density has reached a stable value through sufficient iterations.

2.3. Model validation

Fig. 2left) shows the experimental platform applied for the DMFC testings in present study. The methanol solution composed by deionized water and pure methanol is transported by the peristaltic pump (BT300LC) into the DMFC anode, while an air compressor (OUTSTANDING OTS-550) regulated by a rotameter (OMEGA FMA-2605A) is used to pump the air into the cathode. Operating temperature is manipulated using a supplementary heating apparatus controlled by temperature controller (Omega CSC32). Real-time monitoring of DMFC performances is realized using an electrochemical workstation (CHI660E). An electronic load device (ITECH it8211) is applied to regulate the current density, with the corresponding voltage output being measured at the same time. The CO_2 generation is constantly measured using a CO_2 concentration detector (JA500-CO2-IR1).

Based on this experimental platform, some preliminary experiments are prepared to collect referential results for numerical model validations. A customised single-cell DMFC with regular serpentin channel is used for these preliminary experiments. It consists of a five-layer MEA sandwiched by graphite end plates. For the MEA with an effective active area of 12.25 cm^2, the catalyst and diffusion layers are sandwiched at both the anode and cathode sides. Specifically, the anode catalyst layer is with 4.0 mg/cm^2 Pt-Ru loading and the cathode catalyst layer is with 4.0 mg/cm^2 Pt-C loading. A regular serpentine channel (σ = 1.0, constant cross-section of 0.8 mm^2) of 22 passes are embedded inside the graphite end plates at both anode and cathode sides.

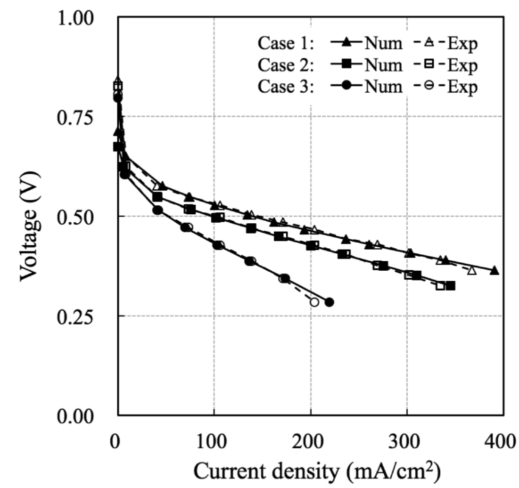

Fig. 3. Comparison of numerical and experimental IV curves at typical operating conditions.

The experiments have been designed to consider four main operating parameters, i.e., temperature (T), input methanol concentration (C_M), methanol flow rate (F_M) and air flow rate (F_A). Fig. 3 shows the comparisons of experimental and numerical IV (current density-voltage) curves at different operating conditions. The main operating parameters (i.e., [T, C_M, F_M, F_A]) are [343.15 K, 0.75 M, 4.5 ccm, 500 ccm], [343.15 K, 1.00 M, 2.0 ccm, 500 ccm] and [313.15 K, 0.75 M, 2.0 ccm, 500 ccm] for Case 1, 2 and 3, respectively. Although the operating conditions vary a lot among the three cases, it can still be noticed that the numerical predications coincide well with experimental IV curves. Such a good agreement between numerical and experimental results has validated the reliability and feasibility of the constructed numerical model.

3. Numerical results and discussions

Effects of non-uniform cross-sectional design on the power generation performances in DMFCs are then investigated using the validated numerical model (see Section 2.2). Concentrating on geometrical effects, numerical simulations of various cross-sectional designs are carried out at the same operating conditions, i.e., T = 343.15 K, C_M = 1.00 M, F_M = 2.0 ccm and F_A = 500 ccm. Comparative studies are then carried out on the numerical results of methanol concentration distributions (Section 3.1), current density distributions (Section 3.2) and current density–voltage relationships (Section 3.3) to clarify the effects

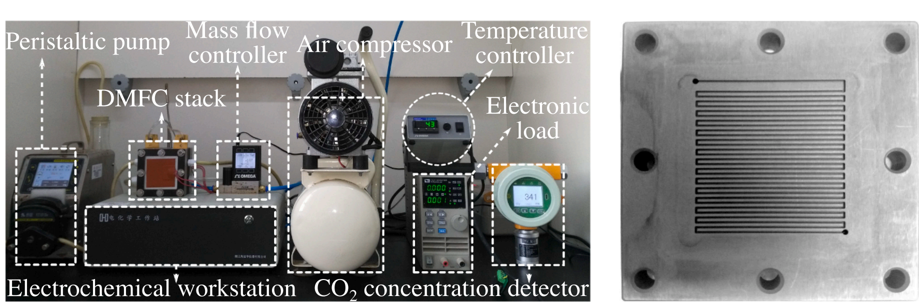

Fig. 2. Experimental platform of a single-cell DMFC system (left) and the regular serpentine channel with uniform cross-section (right).

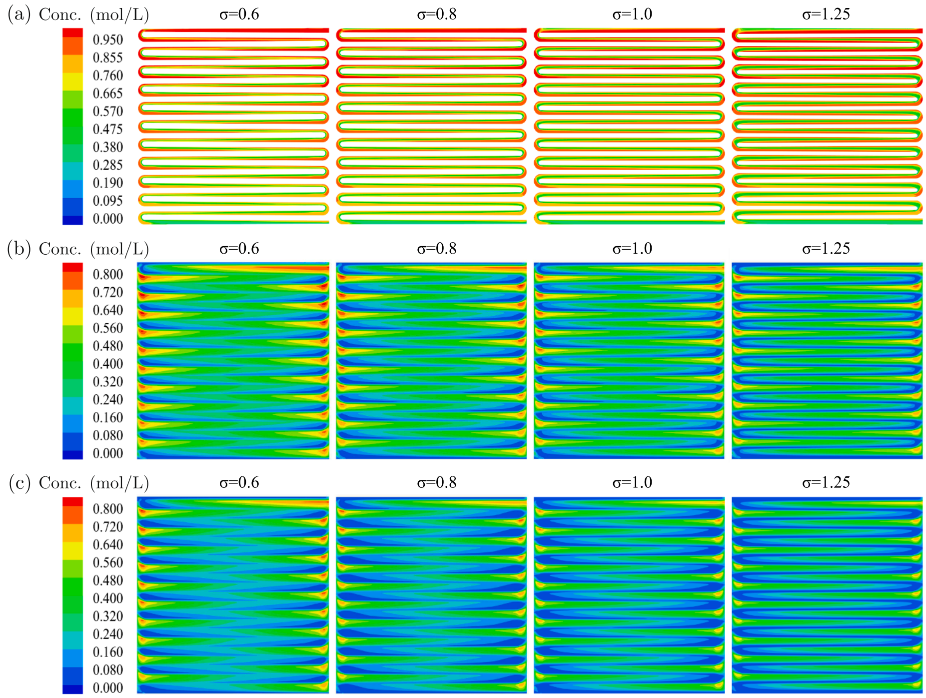

Fig. 4. Methanol concentrations distributing on CD (a), DC (b) and CP (c) planes. The channel inlet is at the top right corner, while the outlet locates at the bottom right.

and mechanisms of non-uniform designs on DMFC performance.

3.1. Methanol concentration distributions

Fig. 4 shows the distributions of methanol concentration on three typical planes inside the DMFC, i.e., the interfaces between the channel and diffusion (CD) layers, the diffusion and catalyst (DC) layers and the catalyst and PEM (CP) layers. On CD plane (Fig. 4(a)), the methanol concentrations for the four designs are all found to be higher at the upstream region than the downstream. This non-uniform distribution coincides well with the physical predication that the methanol fuel is gradually diffused and consumed during its transportation along the flow channel [14,30]. Attributing to the porous structure of diffusion and catalyst layers that allows methanol to diffuse and fulfill in- and through-plane transportations, the striped-like distributions of methanol concentrations can be observed on both DC and CP planes (Fig. 4(b) and (c)). Moreover, successive decrease of methanol concentrations can be noticed from CD to DC and to CP plane, which mainly lies in the effects of fuel consumption and methanol crossover. As the above numerical revealing coincides well with previous literatures [12,13,22], it can validate to some extent the rationality and reasonability of the present numerical results.

With the increase of σ, the overall colour for each planar distribution of methanol concentration on DC and CP planes is observed to become decreasingly bright in Fig. 4(b) and (c). It could come out from the varying pressure drops in different serpentine configurations [34,35]. The pressure drop is found to be 701.3 Pa for $\sigma = 0.6$ but only 325.2 Pa for $\sigma = 1.25$ (see Fig. B.10left) in B). The larger pressure drop in converging channel ($\sigma < 1$) than in diverging one ($\sigma > 1$) could give birth to an enhanced through-plane methanol transportation. Therefore, a relatively small σ can be beneficial for the through-plane methanol transportation from channel layer to the catalyst layer.

Moreover, the accumulation of methanol concentration at the regions near U-turns on DC and CP planes is also found to be enhanced for the decrease of σ, as shown in Fig. 4(b) and (c). It lies in the specific design of cross-sectional recovery at the U-turns, as described in Section 2.1. This specific design requires the channel geometry to be recovered at the U-turns, i.e., the straight converging sections are connected by diverging U-turns (or vice versa). Therefore, the effect of flow deceleration at U-turns can be much more significant with a decrease of σ, as we have found the largest decline of flow velocity among the four designs being at the U-turns with $\sigma = 0.6$, which is about 57% as the velocity magnitude decreases from 0.1 m/s to 0.043m/s (see Fig. B.10right) in B). As flow deceleration normally means depressed species transport and enhanced material accumulation, the specifically designed U-turns thus become the highly-inclined destinations for the in-plane methanol transportations, especially when σ is designed to be small as 0.6.

Summarily speaking, both the in- and through-plane methanol transportations can be enhanced by the decrease of σ. Although an enhanced through-plane transportation usually improves power generations [12,16,17], the accumulated methanol concentration near U-turns (caused by in-plane transportation) might also degrade the planar distribution uniformity, which is usually considered undesirable for efficient power generations [22,34]. Further investigations about the effects of σ on DMFC output performances are still needed.

3.2. Current density distributions

Current density distributing on the CP plane are shown in Fig. 5. Striped-like distributions have been experienced in local current densities for all the four $\sigma = 0.6$, 0.8, 1.0 and 1.25. They are very similar to the methanol concentration distributions as shown in Fig. 4(c). It coincides with the well-recognized fact that the current generation is positively correlated to local methanol concentration [34]. Moreover, the overall color for planar distributions of current densities is found to become increasingly bright as the σ is gradually diminished from 1.25 to 0.6. This result implies that the current generation can be enhanced by the decrease of σ at this given operating condition.

Quantitative analysis was also performed to better understand the mechanism of non-uniform cross-sectional designs. Facet average of current density distribution on the CP plane, as well as the corresponding standard deviation, are summarized in Table 3. They are both observed to gradually augment with the decrease of variation ratio σ. It indicates that the reduction of σ, which was shown to improve the

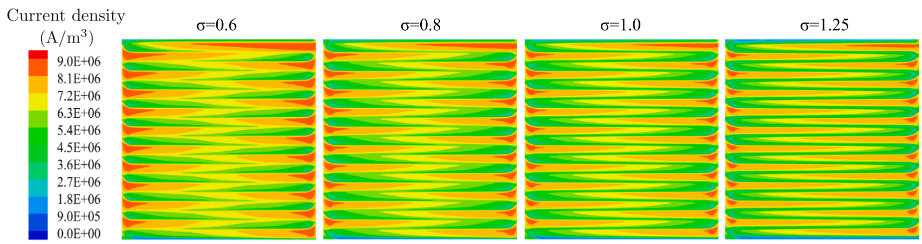

Fig. 5. Current densities distributing on CP plane.

Table 3
Facet average and standard deviation of current densities distributing on CP plane.

Variation ratio (σ)	Facet average (A/m^3)	Standard deviation (A/m^3)
0.6	4.4353×10^6	6.2331×10^5
0.8	4.2288×10^6	7.0629×10^5
1	4.1850×10^6	7.2879×10^5
1.25	4.1119×10^6	8.3661×10^5

through-plane methanol transportation in Section 3.1, has effectively enhanced the power generation performance in the DMFC with serpentine configuration. Moreover, the standard deviation that is suppressed by σ reduction indicates an improved uniformity of current density distribution. As gas production is often in direct proportion to the current generation, this result also implies an uniform gas generation on the catalyst layer for σ reduction, which could be beneficial for operation stability and system. The effectiveness of σ reduction in current generation performance has thus been validated in these numerical results.

3.3. Power generation performances

Effects of non-uniform cross-sectional designs on the global performance of power generation in DMFCs can be well described using IV (current density-voltage) and IP (current density-power density) curves [32,34]. Corresponding to the same operating conditions as applied in Section 3.1 and 3.2, the numerical predications of IV and IP curves obtained with different variation ratio σ are shown in Fig. 6. At low current density (<250 mA/cm^2), the IV/IP curves for different σ are adjacent to each others, but the difference becomes increasingly large as the operating current density continues growing. This result coincides well with previous revealings that the effect of flow-filed designs could be indistinctive at low-current-density operations [8,10,27]. However, for high current density ($\geqslant$ 250 mA/cm^2), the power generation performances (both the voltage and power density) are shown to be

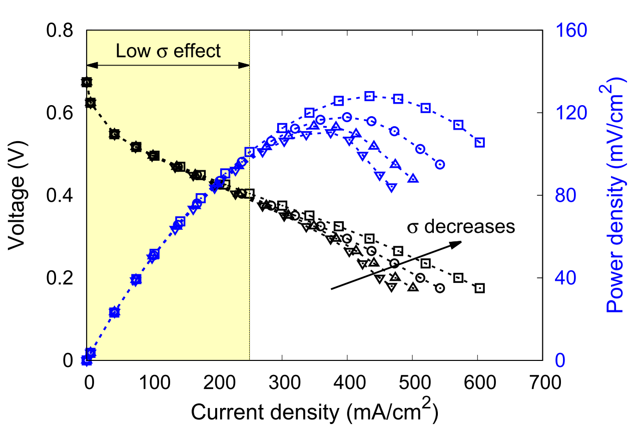

Fig. 6. Effects of non-uniform cross-sectional design on IV and IP curves. Variation ratio σ varies from 0.6 to 0.8 to 1.0 and to 1.25.

effectively enhanced by the reduction of σ. It indicates that the non-uniform cross-sectional design with $\sigma < 1$ can be an effective approach for the enhancements of power generation performances, especially when the DMFC system is required to be operated at high current densities.

4. Experimental validations

To further validate the numerical revealings, systematic experiments based on non-uniform serpentine configuration are discussed in this section. Experimental setup is summarised in Section 4.1. Thereafter, experimental investigations of non-uniform geometric effects on the IV and IP curves are presented in Section 4.2. Power generation performances of non-uniform design at various operating conditions are also carefully examined in Section 4.3 to discuss about the optimal application conditions.

4.1. Experimental setup

Effects of non-uniform serpentine design on cell performances are experimentally investigated based on the experimental platform as presented in Fig. 2left). The regular serpentine channel ($\sigma = 1.0$) that has been presented in Section 2.3 is applied as reference case. Although the maximum performance enhancement is numerically determined to be achieved under an extremely low $\sigma = 0.6$ (see Fig. 6), the non-uniform case for experimental tests is still selected to be with a relatively low $\sigma = 0.8$, to avoid potential practical difficulties in machinability and assembling operations [36]. This non-uniform serpentine channel takes the same pass number, depth, length and inlet area as the regular one. More precisely, its takes 22 passes and its depth is kept at 1.00 mm, while its width is designed to decrease from 0.85 to 0.68 mm in straight sections.

Taking advantages of a digital microscope (VHX-1000 series), the microscope photographs of the manufactured non-uniform channel in graphite end plate can be obtained, as shown in Fig. 7. The divergent design in straight sections, as well as the cross-sectional recovery in U-turns, have been both clearly demonstrated in these 100-times magnified photographs. In experiments, this non-uniform serpentine design is applied as the anode flow channel in the customised single-cell DMFCs as mentioned in Section 2.3. Four main operating parameters, i.e., temperature (T), input methanol concentration (C_M), methanol flow rate (F_M) and air flow rate (F_A) have been considered, which are designed to lie in the following ranges, $T = [298.15, 343.15]$ K, $C_M = [0.75, 1.5]$ M, $F_M = [1.5, 4.5]$ ccm and $F_A = [400, 500]$ ccm.

4.2. IV and IP curves

For comprehensive validations, experiments based on the regular and non-uniform designs are firstly performed at the same operating conditions as numerical simulations, i.e., $T = 343.15$ K, $C_M = 1.00$ M, $F_M = 2.0$ ccm and $F_A = 500$ ccm. Extended experiments are then carried out for different $C_M = 0.5$, 1.5 and 2.0 M, with the other three parameters being fixed, to further study the

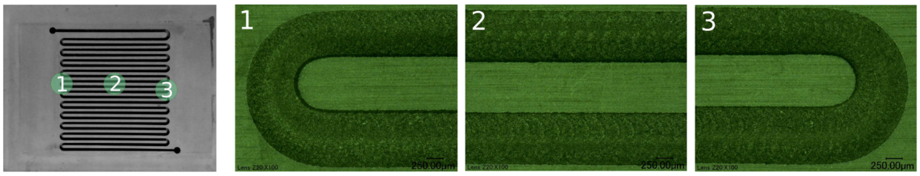

Fig. 7. Microscope photographs of non-uniform cross-sectional designed flow channels.

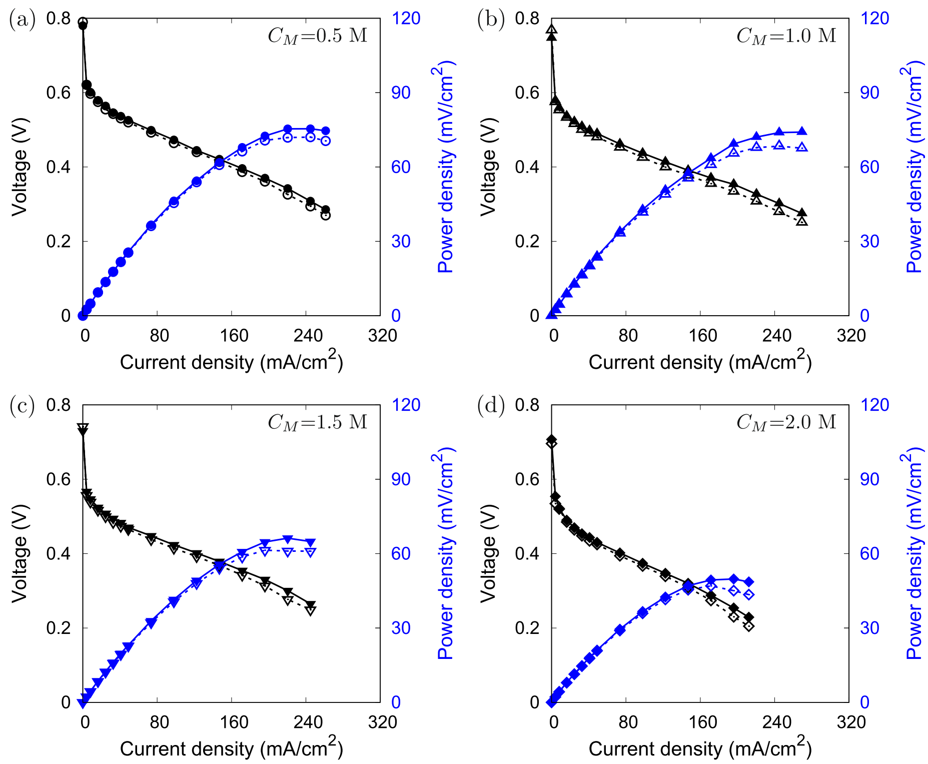

Fig. 8. Effects of input methanol concentrations on the output voltage and power density. Solid-lines: non-uniform channel (σ = 0.8), Dashed-lines: regular channel (σ = 1.0).

effectiveness of non-uniform design under varied operational conditions. The IV and IP curves obtained from above experiments are shown in Fig. 8.

For a low methanol concentration of C_M = 0.5M (Fig. 8(a)), the IV/IP curves obtained in regular and non-uniform designs are almost superimposed at low current densities ($\leqslant$ 160 mA/cm^2). But as the current density grows, the difference between two designs becomes increasingly distinguishable. Similar phenomena can be also revealed in experiments of different methanol concentrations. This result, which coincides well with numerical revealings in Section 3.3, could validate the effectiveness of non-uniform designs in high-current–density operations. Moreover, comparisons among the four cases show that the DMFC performance has been depressed by an increase of C_M exceeding 1.0 M, which could lie in the effects of methanol crossover and/or MEA degradations [37,38]. However, the advantages of non-uniform design over regular one have also been strengthened by the increase of C_M. It has implied the necessity of non-uniform designs in extreme DMFC operations, especially in some potential applications that a high methanol concentration has to be encountered.

4.3. Power generation enhancement

Quantitative analyses are performed based on experimental IP curves, to accurately assess the power generation enhancement imposed by non-uniform design. The growth ratio of power density (η) between the non-uniform and regular designs is defined as,

$$\eta_j = \frac{P_{Nj} - P_{Rj}}{P_{Rj}}, \tag{2}$$

where j denotes the operating current density, P_{Nj} and P_{Rj} represent the power densities at j generated by non-uniform and regular channels, respectively. The determined power generation enhancement (η) at various operating conditions are presented in Fig. 9.

Fig. 9(a) corresponds to the experiments in Section 4.2 that are designed to consider the effects of input methanol concentrations. All the power density enhancements (η) are observed above 0%, despite of the variation of methanol concentrations. It indicates that the non-uniform design (σ = 0.8) could always generate positive effects on the power generations. Especially when the current density exceeds 160 mA/cm^2, the power generation enhancements increase at accelerate rates for all the four methanol concentrations. Taking C_M = 1.0 M for instance, the non-uniform cross-sectional design (σ = 0.8) has generated a considerable power density enhancement above 4% when the operating current density becomes larger than 160 mA/cm^2, and it could even reach about 9.6% at 269 mA/cm^2. It is also encouraging to discover that, the case of C_M = 1.0 M experiences the largest power density enhancement above 147 mA/cm^2, even if its power output is relatively low among the four cases in Fig. 8. It implies that the negative effects of methanol crossover and MEA degradation could be largely depressed by this non-uniform design, which is found to be able to distribute methanol concentrations (and generated current densities) more uniformly inside DMFCs (see Section 3.1 and 3.2). The necessity of non-uniform designs in extreme DMFC operations has thus been further validated.

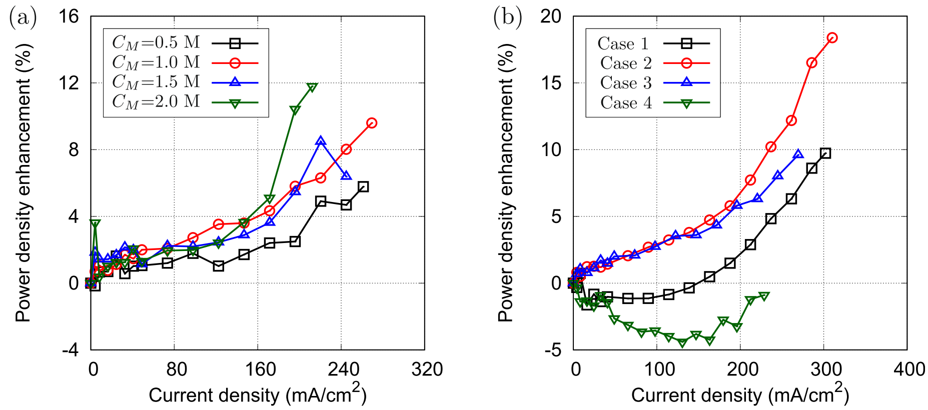

Fig. 9. Power generation enhancement by the non-uniform cross-sectional designs (σ = 0.8).

Table 4
Supplementary experiments for consideration of multi-parameter variations.

No.	T (K)	C_M (M)	F_M (ccm)	F_A (ccm)
1	343.15	0.75	3.5	500
2	343.15	0.75	4.5	500
3	343.15	1.00	2.0	500
4	328.15	0.75	2.0	500

Compared with experiments in Section 4.2 that only concern about single-parameter effects (input methanol concentration), some supplementary experiments are provided to further investigate the effects of multiple operating parameter variations. Differences in operating temperature, methanol concentration and methanol flow rates are considered (Table 4), other than the anode air flow rate that is normally sufficient in DMFC operations. Fig. 9(b) shows the power density enhancement analyses on the IP curves obtained from these supplementary experiments. For Case 1, the power generation is found to be enhanced by non-uniform design at high current densities (i.e., $\eta > 0\%$ for $j > 164$ mA/cm^2), and it achieves an average enhancement of about $\eta = 4.9\%$ at the current density range of [163.3, 302.0] mA/cm^2. More encouraging enhancements of power generations can be noticed for Case 2 and 3. Especially for Case 3, it experiences an average enhancement of about $\eta = 10.8\%$ in the current density range of [163.3, 310.2] mA/cm^2, and a significant enhancement of $\eta = 18.4\%$ can be fulfilled at 310.2 mA/cm^2. However, this non-uniform design ($\sigma = 0.8$, converging channel) could also generate unfavorable effects in power generation, e.g., the low-current-operations in Case 1. Moreover, the power generation is found to be always depressed for $\eta < 0\%$ in Case 4 in which a relatively low operating temperature is imposed. The above results remind us that this non-uniform design of converging channel ($\sigma = 0.8$) could be specifically beneficial for power generation enhancements in high-current-density DMFC operations at high operating temperatures.

5. Conclusions

Effects of non-uniform cross-sectional designs on the power generation performance in DMFCs with serpentine configurations are systematically investigated in the present study. A parametric design was proposed to describe and classify different channel geometries. The underlying mechanisms and the optimal application conditions of non-uniform cross-sectional designs have been carefully analyzed using numerical and experimental techniques. The main findings in the present study can be summarized as follows,

1)Converging channels ($\sigma < 1.0$) in non-uniform cross-sectional designs are numerically shown to be beneficial for both in- and through-plane methanol transportations, which yields the uniformity-improved distributions of methanol concentration and current density at typical DMFC operating conditions. Considerable enhancement in power generation performances has also been revealed from numerical IV/IP curves as a result of σ reduction, especially in high-current-density operations.

2)Effectiveness of converging designs for power generation enhancements has also been validated by experimental studies. Non-uniform converging design ($\sigma = 0.8$) is proposed to be beneficial for the depression of methanol crossover and MEA degradation. Specifically, a considerable power generation enhancement of about $4 - 12\%$, which is quantified from experimental data, have thus been noticed at the operating current density range of [160, 269] mA/cm^2 for this machined converging design ($\sigma = 0.8$).

3)More significant enhancement of power generation (18.4%) has also been achieved using converging design ($\sigma = 0.8$) in experiments of multi-operating-parameter variations. Non-uniform converging designs are proposed to be highly beneficial for power generation enhancements in high-current–density DMFC operations at high operating temperatures. However, special attention is also proposed to be paid on low-temperature conditions, in which the power generation enhancement by the usage of converging design could cease to be effective. It suggests subsequent studies on the coupling effects of cross-sectional designs and operating conditions.

Declaration of interest

None declared.

Acknowledgments

Project supported by the National Natural Science Foundation of China (Nos. 51505136 & 11402084), the Natural Science Foundation of Hunan Province (Nos. 2017JJ3018 & 2015JJ3051), the China Scholarship Council (No. 201806135023) and the open fund of State Key Laboratory of Fluid Power & Mechatronics Systems (No. GZKF-201615).

Appendix A. Relevant governing equations in numerical models

Governing equations that are applied in our numerical models are as follows,

1Continuity equation (mass conservation):

$$\vec{\nabla}\cdot(\varepsilon\rho\vec{v}) = S_m, \tag{3}$$

where ε is the porosity of physical domain, ρ is the mixture density, $\vec{v}$ is the velocity of mixture and S_m is the mass source term.
2Momentum conservation equation:

$$\vec{\nabla}\cdot(\varepsilon\rho\vec{v}\vec{v}) = -\vec{\nabla}(\varepsilon P) + \nabla^2(\varepsilon\mu\vec{v}) + S_{mon}, \tag{4}$$

where P denotes the pressure, μ is mixture viscosity and S_{mom} denotes the momentum source term caused by the resistance of porous media.
3Species transport equations:

$$\vec{\nabla}\cdot(\varepsilon\rho\vec{v}y_k) = \vec{\nabla}\cdot(\varepsilon\rho D_k^{eff}\vec{\nabla}y_k) + S_m, \tag{5}$$

where y_k denotes the mass fraction of specie k and D_k^{eff} denotes the effective diffusion coefficient of specie k.
4Electro-chemical expression (local volumetric current density):

$$j_a = \frac{E_0 - E_{cell} - \eta_a - \eta_c}{t_{acl}R_{mem}}, \tag{6}$$

where E_0 is the open circuit voltage, E_{cell} is the cell potential, t_{acl} is the thicknesses of catalyst layer and R_{mem} represents the area specific resistance of membrane. The over-potential values at anode and cathode sides, η_a and η_c, are derived from semi-empirical equations.

Appendix B. Variations of flow pressure and velocity magnitude along the flow channels

Fig. B.10

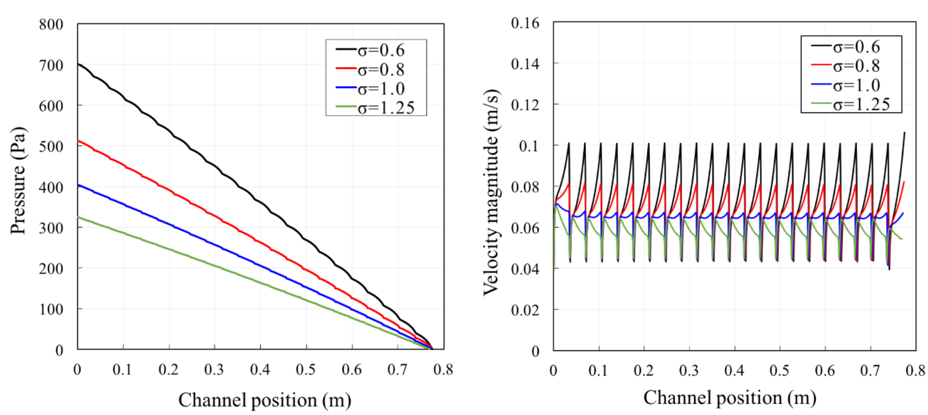

Fig. B.10. Variations of flow pressure (left) and velocity magnitude (right) along the flow channels. Channel position denotes the axial position of the flow channel, i.e., 0 m for inlet and 0.775 m for outlet.

References

[1] Sharaf OZ, Orhan MF. An overview of fuel cell technology: fundamentals and applications. Renew Sustain Energy Rev 2014;32:810–53.
[2] Munjewar S, Thombre S, Mallick R. Approaches to overcome the barrier issues of passive direct methanol fuel cell – review. Renew Sustain Energy Rev 2017;67:1087–104.
[3] Patel P, Datta M, Jampani P, Hong D, Poston J, Manivannan A, Kumta P. High performance and durable nanostructured TiN supported Pt_{50}–Ru_{50} anode catalyst for direct methanol fuel cell (DMFC). J Power Sources 2015;293:437–46.
[4] Wang M, Liu G, Tian Z, Shao Y, Wang L, Ye F, Tran M, Yun Y, Lee J. Microstructure-modified proton exchange membranes for high-performance direct methanol fuel cells. Energy Convers Manage 2017;148:753–8.
[5] Mehmood A, An M-G, Ha H. Physical degradation of cathode catalyst layer: a major contributor to accelerated water flooding in long-term operation of DMFCs. Appl Energy 2014;129:346–53.
[6] Yuan W, Wang A, Ye G, Pan B, Tang K, Chen H. Dynamic relationship between the CO_2 gas bubble behavior and the pressure drop characteristics in the anode flow field of an active liquid-feed direct methanol fuel cell. Appl Energy 2017;188:431–43.
[7] Nguyen T. A gas distributor design for Proton-Exchange-Membrane fuel cells. J Electrochem Soc 1996;143(5):L103–5.
[8] Wong C, Zhao T, Ye Q, Liu J. Experimental investigations of the anode flow field of a micro direct methanol fuel cell. J Power Sources 2006;155(2):291–6.
[9] Jung G-B, Su A, Tu C-H, Weng F-B, Chan S-H. Innovative flow-field combination design on direct methanol fuel cell performance. J Fuel Cell Sci Technol 2007;4(3):365–8.
[10] Hsieh S-S, Wu H-C, Her B-S. A novel design for a flow field configuration of a direct methanol fuel cell. J Power Sources 2010;195(10):3224–30.
[11] Lu Y, Reddy R. Effect of flow fields on the performance of micro-direct methanol fuel cells. Int J Hydrogen Energy 2011;36(1):822–9.
[12] Ozden A, Ercelik M, Ouellette D, Colpan C, Ganjehsarabi H, Hamdullahpur F. Designing, modeling and performance investigation of bio-inspired flow field based DMFCs. Int J Hydrogen Energy 2017:1–13.
[13] Ouellette D, Ozden A, Ercelik M, Colpan C, Ganjehsarabi H, Li X, Hamdullahpur F. Assessment of different bio-inspired flow fields for direct methanol fuel cells through 3D modeling and experimental studies. Int J Hydrogen Energy 2018;43(2):1152–70.
[14] Arico A, Cretí P, Baglio V, Modica E, Antonucci V. Influence of flow field design on the performance of a direct methanol fuel cell. J Power Sources 2000;91(2):202–9.
[15] Wang S-J, Huo W-W, Zou Z-Q, Qiao Y-J, Yang H. Computational simulation and experimental evaluation on anodic flow field structures of micro direct methanol fuel cells. Appl Therm Eng 2011;31(14–15):2877–84.
[16] Deng H, Sang S, Zhang Y, Li Z, Liu X. Investigations of silicon-based air-breathing micro direct methanol fuel cells with different anode flow fields. Microelectron Eng

2013;111:180–4.
[17] Wu Y, Cho J, Neville T, Meyer Q, Zeische R, Boillat P, Cochet M, Shearing P, Brett D. Effect of serpentine flow-field design on the water management of polymer electrolyte fuel cells: an in-operando neutron radiography study. J Power Sources 2018;399:254–63.
[18] Yang H, Zhao T. Effect of anode flow field design on the performance of liquid feed direct methanol fuel cells. Electrochim Acta 2005;50(16–17):3243–52.
[19] Vijayakumar R, Rajkumar M, Sridhar P, Pitchumani S. Effect of anode and cathode flow field depths on the performance of liquid feed direct methanol fuel cells (DMFCs). J Appl Electrochem 2012;42(5):319–24.
[20] Chang D-H, Wu S-Y. The effects of channel depth on the performance of miniature proton exchange membrane fuel cells with serpentine-type flow fields. Int J Hydrogen Energy 2015;40(35):11659–67.
[21] Kianimanesh A, Yu B, Yang Q, Freiheit T, Xue D, Park S. Investigation of bipolar plate geometry on direct methanol fuel cell performance. Int J Hydrogen Energy 2012;37(23):18403–11.
[22] Park Y-C, Chippar P, Kim S-K, Lim S, Jung D-H, Ju H, Peck D-H. Effects of serpentine flow-field designs with different channel and rib widths on the performance of a direct methanol fuel cell. J Power Sources 2012;205:32–47.
[23] Manso A, Marzo F, Mujika M, Barranco J, Lorenzo A. Numerical analysis of the influence of the channel cross-section aspect ratio on the performance of a PEM fuel cell with serpentine flow field design. Int J Hydrogen Energy 2011;36(11):6795–808.
[24] Tafaoli-Masoule M, Bahrami A, Elsayed E. Optimum design parameters and operating condition for maximum power of a direct methanol fuel cell using analytical model and genetic algorithm. Energy 2014;70:643–52.
[25] Sudaroli B, Kolar A. Experimental and numerical study of serpentine flow fields for improving direct methanol fuel cell performance. Fuel Cells 2015;15(6):826–38.
[26] Jung S, Wang C-Y. Direct methanol fuel cells with streamline graded structure under ultra-low fuel stoichiometry condition. J Power Sources 2014;248:253–64.
[27] Chowdhury M, Akansu Y. Novel convergent-divergent serpentine flow fields effect on PEM fuel cell performance. Int J Hydrogen Energy 2017;42(40):25686–94.
[28] Seyhan M, Akansu Y, Murat M, Korkmaz Y, Akansu S. Performance prediction of PEM fuel cell with wavy serpentine flow channel by using artificial neural network. Int J Hydrogen Energy 2017;42(40):25619–29.
[29] Zehtabiyan-Rezaie N, Arefian A, Kermani M, Noughabi A, Abdollahzadeh M. Effect of flow field with converging and diverging channels on proton exchange membrane fuel cell performance. Energy Convers Manage 2017;152:31–44.
[30] Hu X, Wang X, Chen J, Yang Q, Jin D, Qiu X. Numerical investigations of the combined effects of flow rate and methanol concentration on DMFC performance. Energies 2017;10(8):1094.
[31] Yang Q-W, Hu X-Q, Lei X-C, Zhu Y, Wang X-Y, Ji S-C. Adaptive operation strategy for voltage stability enhancement in active DMFCs. Energy Convers Manage 2018;168:11–20.
[32] Yang Q-W, Hu X-Q, Zhu Y, Lei X-C, Yu B, Ji S-C. Extended criterion for robustness evaluations of energy conversion efficiency in DMFCs. Energy Convers Manage 2018;172:285–95.
[33] Yousefi S, Zohoor M. Conceptual design and statistical overview on the design of a passive DMFC single cell. Int J Hydrogen Energy 2014;39(11):5972–80.
[34] Li X, Sabir I. Review of bipolar plates in PEM fuel cells: Flow-field designs. Int J Hydrogen Energy 2005;30(4):359–71.
[35] Duryodhan V, Singh S, Agrawal A. Liquid flow through converging microchannels and a comparison with diverging microchannels. J Micromech Microeng 2014;24(12):125002 .
[36] Cheng Q, Zhao H, Zhao Y, Sun B, Gu P. Machining accuracy reliability analysis of multi-axis machine tool based on monte carlo simulation. J Intell Manuf 2018;29(1):191–209.
[37] Yang Q, Kianimanesh A, Freiheit T, Park S, Xue D. A semi-empirical model considering the influence of operating parameters on performance for a direct methanol fuel cell. J Power Sources 2011;196(24):10640–51.
[38] Nam K, Lim S, Kim S, Yoon S, Jung D. Application of silica as a catalyst support at high concentrations of methanol for direct methanol fuel cells. Int J Hydrogen Energy 2012;37(5):4619–26.